

Peristaltic Transport of Ellis Fluid under the Influence of Viscous Dissipation Through a Non-Uniform Channel by Multi-Step Differential Transformation Method

Asha. S. Kotnurkar^{1,*}, Joonabi Beleri¹

¹ Department of Studies and Research in Mathematics, Karnatak University, Dharwad-580003, India

ABSTRACT

The current work is investigating the influence of viscous dissipation on Ellis fluid in peristaltic flow through a rough non-uniform channel. The non-linear relationship between shear stress and strain rate is demonstrated by the Ellis liquid model. Dissipation is the process of converting downward-flowing water's mechanical energy into thermal and acoustic energy. Using appropriate non-dimensional parameters, the governing equations are transformed into conventional non-linear partial differential equations. The Multi-Step Differential Transformation Method is used to find solutions to developing equations. Velocity near the center of the channel enhances with rising an Ellis fluid parameter, on the contrary, it follows the inverse trend near the channel wall. Temperature distribution diminishes when there is a rise in Brinkman number. Temperature distribution enhances when there is a rise in Ellis fluid parameter. As an Ellis fluid parameter rises the concentration profile diminishes. Solutal concentration profile in peristaltic pumping increases by rising the values of Brinkman number. The influence of surface roughness in flow of physiological liquids is much helpful in understanding different problems related to blood transport in coronary arteries. surface roughness attracted the interest of scientist in chemical engineering to understand the significance of roughness of wall formed as an effect of chemical erosion during flow of chemicals. Graphs depict the influence of several parameters on velocity, concentrations, temperature, and streamlines.

Keywords:

Peristaltic flow; Ellis fluid; Viscous
Dissipation; Rough surface; Non-Uniform
channel; Ms-DTM

Received: 8 March 2022

Revised: 21 April 2022

Accepted: 21 April 2022

Published: 13 May 2022

1. Introduction

Nowadays, Peristaltic transport is one of the most important pumping mechanisms due to its vast engineering, medical sciences, and biomechanics appliances. The mechanism of peristalsis is due to a wave transmission along the tube wall or channel. The word "peristalsis" is derived from the Greek word "Peristaltikos", meaning clasp and compression. In 1966 Latham [1] introduced the Peristalsis. Peristalsis is the principle behind many devices, including heart-lung machines, finger and roller pumps. The processes of oxygenation and hemodialysis are also biologically significant. Further, Shapiro *et al.*, [2] analysed the mechanism of peristaltic at low Reynolds number with long wavelengths. Jaffrin *et al.*, [3] demonstrated the mechanism of peristaltic motion in Newtonian and non-Newtonian liquids. Non-Newtonian fluid transport phenomena have increased considerably due

* Corresponding author.
E-mail address: ashask@kud.ac.in

to their importance in biological and industrial applications. A non-Newtonian fluid model has a non-linear relationship between shear stress and shear rate. Examples of non-Newtonian liquids are polymer solution, ketchup, paint, colloids gel, custard, starch suspension, molten polymer, toothpaste shampoo, and blood. An important class of these non-Newtonian fluids constitutes the linear viscoelastic model. The reference [4-5] describes how researchers investigated the peristaltic transport of fluids in various geometrical configurations. Shapiro *et al.*, (1969) discovered trapping theoretically. Trapping can be defined as the region of closed stream lines in the wave frame at high flow rates and large conclusions. The streamlines split under certain conditions, forming a recirculating closed streamline region. The wave traps the laboratory frame in this region as it advances with the wave speed. This is known as "trapping."

Longwell [6] studied the transport of an Ellis liquid with an impermeable wall through a circular tube (1966). The Ellis model combines the power-law and Bingham (viscoplastic) models into a single model. The non-linear relationship between shear stress and strain rate is demonstrated by the Ellis liquid model. At high shear stresses, it acts like a power-law model, and at low shear stresses, it acts like a Newtonian model. The flowing liquid involves water, corrosive or abrasive, shear thickening elements like oxidizers and gels. Shear-thinning elements like polymer solutions and paints. The Power-law model is a motion behaviour that simulates shear-thinning and/or shear thickening liquids. When significant departures from the model are observed at low shear rates, the Ellis model is appropriate. Due to the power-law liquid model's limiting value behaviour, Ellis proposed a three-parameter liquid model that switched the roles of shear stress and strain rates to show transport characteristics over small shear rate ranges.

Surface roughness is one of the components of surface texture. The roughness is seen as minute irregularities in the surface texture that emerge throughout the production process. The effects of surface roughness were first analyzed by Nikuradse (1933). Surface roughness is assumed along the surface of geometry and is modelled as a sine waveform; that is, the roughness over the surface is mathematically modelled as a sinusoidal waveform having a high frequency and low amplitude. Influence of surface roughness in flow of physiological liquids is much helpful in understanding different problems related to blood transport in coronary arteries. Mechanism of biofluids have small degree of roughness or uncertain spatial variability in Biological organs. Influence on transport because of surface roughness attracted the interest of scientist in chemical engineering to understand the significance of roughness of wall formed as an effect of chemical erosion during flow of chemicals. Due to its wide range of appliances in engineering, studying the influence of wall roughness while considering roughness orientation, roughness structure, and roughness element shape has become a key area of research. Shukla *et al.*, [15,16] demonstrated the effect of rough surface in peristaltic flow through non-uniform inclined channel. Burton *et al.*, [17] analysed the surface roughness of the coronary arteries. Taylor *et al.*, [18] studied Characterization of the effect of surface roughness. Viscous dissipation changes the temperature distributions by playing a role like energy source, which leads to affect heat transfer rates. Dissipation is the process of converting downward-flowing water's mechanical energy into thermal and acoustic energy. Shaheen *et al.*, [19] explained influence of convectively heated surface with viscous dissipation on sisko fluid. Mehmood *et al.* [20] demonstrated impact of viscous dissipation in peristaltic flow. Abou-Zeid *et al.*, [21] studied viscous dissipation on peristaltic motion of micropolar non-Newtonian nano liquid.

In the view of the above literature, the current study shows the application of viscous dissipation and rough surface effects in peristaltic Ellis fluid movement through non-uniform channel mathematically. In recent years, there has been a surge of inattentiveness in developing and applying analytical and numerical approaches. Such strategies can aid in overcoming the complexity and non-

linearity seen in non-Newtonian liquids. Mechanism of peristaltic with non-Newtonian liquid necessitates substantially non-linear partial differential equations. It is hard to find precise answers to such challenges. We employed a semi-analytical technique known as the Differential Transform Method (DTM) in this research. In 1986, Zhou was the first to introduce DTM [22]. The Multi-Step Differential Transformation Approach (Ms-DTM) is a dependable semi-analytical method that is an excellent enhancement over the traditional DTM. Furthermore, Odibat *et al.*, [23] demonstrated the Ms-DTM and its appliances to chaotic or non-chaotic systems. Further work is carried out by Hasona *et al.*, [24-26], Tripathi *et al.*, [27], Hatami *et al.*, [28], Beg *et al.*, [29] and Asha *et al.*, [30-31] for solving non-linear ODE and PDE.

In sight of these appliances, the objective of this study is to provide different predictions about the effect of viscous dissipation features and rough surface on the peristalsis of Ellis fluid through a non-uniform channel. Ms-DTM is used to solve nonlinear governing equations and physical parameters' temperature, concentration, and velocity are debated through graphs.

2. Construction of governing equations

Consider an Ellis fluid peristaltic motion in a two-dimensional non-uniform channel propagating the sinusoidal wave towards its rough surface walls. Take the Cartesian coordinate system (\tilde{X}, \tilde{Y}) , the physical configuration of the channel wall surface is shown in Fig. 1

$$h(\tilde{X}, \tilde{t}) = d(\tilde{X}) + b \sin\left(\frac{2\pi}{\lambda}(\tilde{X} - c\tilde{t})\right) - b_1 \cos^4\left(\frac{\pi\tilde{X}}{\lambda_1}\right) \quad \text{with} \quad d(\tilde{X}) = a + K\tilde{X} \quad (1)$$

here b denotes amplitude of the wave, a denotes half channel width, λ denotes length of wave, c denotes velocity propagation, \tilde{t} denotes time, K denotes the non-uniformity parameter, b_1 represents the height of roughness, λ_1 represents the pitch and \tilde{X} represents the axial variable.

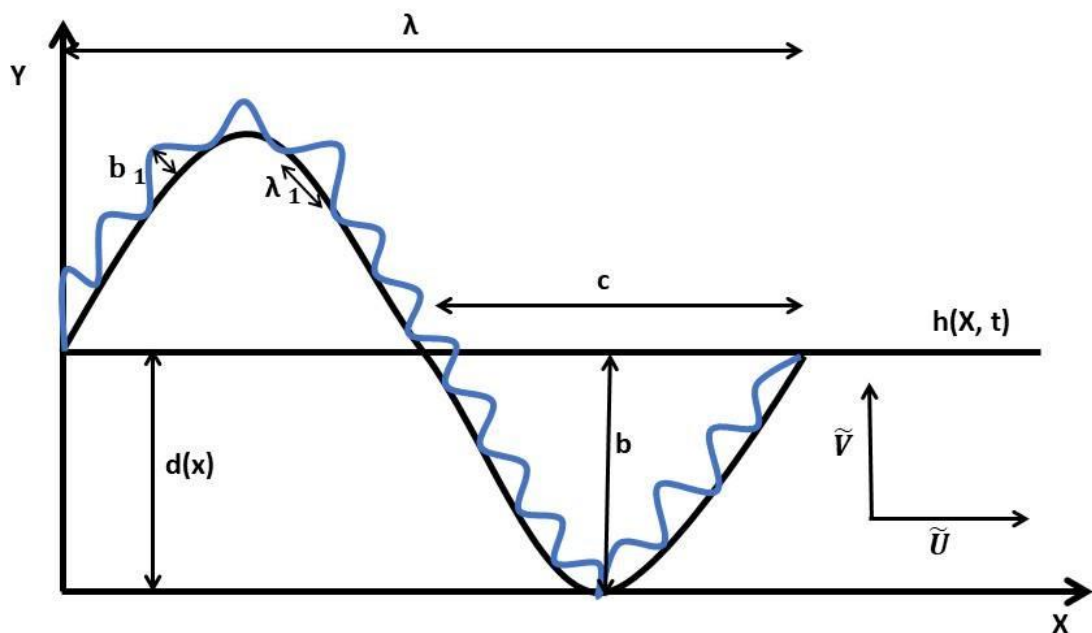


Figure 1: Physical Configuration

Let v be the velocity field defined as $v = (\tilde{U}, \tilde{V}, 0)$. (2)

Where \tilde{U} and \tilde{V} are parameters of velocity respectively.

For an Ellis fluid, the constitutive equations between strain and stress is given as [7]

$$S = \mu \frac{A_1}{1 + (\pi_s / \tau_0^2)^{\alpha-1}}, \tag{3}$$

In above equation μ denotes dynamic viscosity, α denotes material constant, A_1 represents first Rivlin-Ericksen tensor, τ defines second order stress tensor invariant. The shear stress (s) that corresponds to half of (μ) is commonly defined as constant τ_0 . For $\alpha = 1$ and $1/\tau_0 \rightarrow 0$ the fluid model (1) turns to Newtonian model.

An Ellis liquid's governing equations [7] are as given below:

$$\frac{\partial \tilde{U}}{\partial \tilde{X}} + \frac{\partial \tilde{U}}{\partial \tilde{Y}} = 0, \tag{4}$$

$$\rho_f \left(\frac{\partial \tilde{U}}{\partial t} + \tilde{U} \frac{\partial \tilde{U}}{\partial \tilde{X}} + \tilde{V} \frac{\partial \tilde{U}}{\partial \tilde{Y}} \right) = -\frac{\partial \tilde{p}}{\partial \tilde{X}} + \frac{\partial \tilde{s}_{\tilde{x}\tilde{x}}}{\partial \tilde{X}} + \frac{\partial \tilde{s}_{\tilde{x}\tilde{y}}}{\partial \tilde{Y}}, \tag{5}$$

$$\rho_f \left(\frac{\partial \tilde{V}}{\partial t} + \tilde{U} \frac{\partial \tilde{V}}{\partial \tilde{X}} + \tilde{V} \frac{\partial \tilde{V}}{\partial \tilde{Y}} \right) = -\frac{\partial \tilde{p}}{\partial \tilde{Y}} + \frac{\partial \tilde{s}_{\tilde{x}\tilde{x}}}{\partial \tilde{X}} + \frac{\partial \tilde{s}_{\tilde{x}\tilde{y}}}{\partial \tilde{Y}}, \tag{6}$$

$$\rho c_p \left(\frac{\partial \tilde{T}}{\partial t} + \tilde{U} \frac{\partial \tilde{T}}{\partial \tilde{X}} + \tilde{V} \frac{\partial \tilde{T}}{\partial \tilde{Y}} \right) = k \Delta^2 \tilde{T} + \tilde{s}_{\tilde{x}\tilde{x}} \frac{\partial \tilde{U}}{\partial \tilde{X}} + \left(\frac{\partial \tilde{U}}{\partial \tilde{X}} + \frac{\partial \tilde{V}}{\partial \tilde{Y}} \right) \tilde{s}_{\tilde{x}\tilde{y}} + \tilde{s}_{\tilde{y}\tilde{y}} \frac{\partial \tilde{V}}{\partial \tilde{Y}} + \frac{\partial \tilde{q}_r}{\partial \tilde{Y}}, \tag{7}$$

$$\frac{\partial \tilde{C}}{\partial t} + \tilde{U} \frac{\partial \tilde{C}}{\partial \tilde{X}} + \tilde{V} \frac{\partial \tilde{C}}{\partial \tilde{Y}} = D \left(\frac{\partial^2 \tilde{C}}{\partial \tilde{X}^2} + \frac{\partial^2 \tilde{C}}{\partial \tilde{Y}^2} \right) + \frac{DK_T}{T_m} \left(\frac{\partial^2 \tilde{T}}{\partial \tilde{X}^2} + \frac{\partial^2 \tilde{T}}{\partial \tilde{Y}^2} \right), \tag{8}$$

Here T_m denotes Fluid mean temperature, $\tilde{s}_{\tilde{x}\tilde{x}}$, $\tilde{s}_{\tilde{x}\tilde{y}}$, $\tilde{s}_{\tilde{y}\tilde{y}}$ defines extra stress tensor components of fluid, K_T is the ratio of thermal diffusion and D represents the mass diffusivity coefficient.

The relationship between the laboratory frame and wave frame is defined by

$$\tilde{u}(\tilde{x}, \tilde{y}) = \tilde{U} - c, \quad \tilde{v}(\tilde{x}, \tilde{y}) = \tilde{V}, \quad \tilde{x} = \tilde{X} - c\tilde{t}, \quad \tilde{y} = \tilde{Y}, \tag{9}$$

where (\tilde{u}, \tilde{v}) are velocity components, (\tilde{x}, \tilde{y}) are coordinates in a wave frame.

The radiative heat flux (\tilde{q}_r) and Fourier law of heat conduction are as below

$$\tilde{q}_r = \left(\frac{-4\sigma}{3k} \right) \frac{\partial}{\partial \tilde{y}} T_f^4, \quad q = -k \Delta T \tag{10}$$

Here σ denotes Stefan-Boltzman constant, k denotes the parameter of the mean absorption coefficient, q represents local heat flux vector and ΔT represents temperature gradient. The temperature of the liquid within the fluid flow was also assumed to be low. By expanding T^4 and T_0 and ignoring higher order terms we obtain

$$T^4 \cong 4T_0^3 T - 3T_0^4 \tag{11}$$

the expression mentioned above and equation (10) gives

$$q_r = \left(\frac{-16\sigma T_0^3}{3k} \right) \frac{\partial}{\partial \tilde{y}} T_f \tag{12}$$

The effects of a compliant wall are defined as $L(P) = P - P_0$ (13)

Where $P_0 = 0$ refers to the pressure on the outside of the channel wall caused by muscle tension. The operator L gives a viscosity damping effect to the strained membrane, which is defined as

$$L = -R \frac{\partial^2}{\partial X^2} + M \frac{\partial^2}{\partial t^2} + N \frac{\partial}{\partial t}$$
 (14)

where $(\tau), (n_1), (m_1)$ are elastic tension in membrane, coefficient of viscous damping effect and plate mass/unit area:

$$\frac{\partial P}{\partial X} = E_1 \frac{\partial^3 h}{\partial X^3} + E_2 \frac{\partial^3 h}{\partial t^2 \partial X} + E_3 \frac{\partial^2 h}{\partial t \partial X}$$
 (15)

where $E_1 = -Ra^3/\mu_s \lambda^3 c$, $E_2 = Ma^3 c/\mu_s \lambda^3$ and $E_3 = Na^3/\mu_s \lambda^2$ represents the non-dimensional parameters.

Introducing quantities with no dimension of interest as below:

$$\left. \begin{aligned} x = \frac{\tilde{x}}{\lambda}, y = \frac{\tilde{y}}{a}, t = \frac{c\tilde{t}}{\lambda}, p = \frac{a^2 \tilde{p}}{c\lambda\mu_s}, v = \frac{\tilde{v}}{c}, u = \frac{\tilde{u}}{c}, h = \frac{\tilde{h}}{a}, \delta = \frac{a}{\lambda}, P_r = \frac{ac_p}{k} \\ R_e = \frac{\rho_f ca}{\mu}, \alpha = \frac{k_r}{(\rho c)_f}, \Omega = \frac{\tilde{C} - \tilde{C}_0}{\tilde{C}_1 - \tilde{C}_0}, \theta = \frac{\tilde{T} - \tilde{T}_0}{\tilde{T}_1 - \tilde{T}_0}, R_d = -\frac{16\sigma\tilde{T}_0^3}{3k\mu c_f}, \lambda_1 = \frac{\tilde{\lambda}_1}{\lambda} \\ S_{\tilde{x}\tilde{x}} = \frac{\mu c}{d} \tilde{S}_{\tilde{x}\tilde{x}}, S_{\tilde{x}\tilde{y}} = \frac{\mu c}{d} \tilde{S}_{\tilde{x}\tilde{y}}, S_{\tilde{y}\tilde{y}} = \frac{\mu c}{d} \tilde{S}_{\tilde{y}\tilde{y}}, B_r = E_c P_r, E_c = \frac{c^2}{c_f(\tilde{T}_1 - \tilde{T}_0)}, \\ S_c = \frac{\gamma}{D_m}, S_r = \frac{\rho D k_r (\tilde{T}_1 - \tilde{T}_0)}{\mu T_m (\tilde{C}_1 - \tilde{C}_0)}, \beta = \frac{c}{a\tau_0^2}, \phi = \frac{b}{a}, \phi_1 = \frac{b_1}{a}, u = \frac{\partial \Psi}{\partial y}, v = -\delta \frac{\partial \Psi}{\partial x} \\ f^* = \frac{q}{ca}, h = \frac{\tilde{h}}{a} = 1 + \frac{K\lambda X}{a} + \phi \sin 2\pi(X - t) - \phi_1 \cos^4\left(\frac{\pi X}{\lambda_1}\right). \end{aligned} \right\}$$
 (16)

Where θ and Ω are the dimensionless temperature and solutal concentration respectively.

$$S_{xx} = \frac{2\delta \frac{\partial u}{\partial x}}{1 + (\beta\chi)^{\alpha-1}}, S_{yy} = \frac{2\delta \frac{\partial v}{\partial y}}{1 + (\beta\chi)^{\alpha-1}},$$
 (17)

$$S_{xy} = \frac{\left(\frac{\partial u}{\partial y} + \delta \frac{\partial v}{\partial x}\right)}{1 + (\beta\chi)^{\alpha-1}},$$
 (19)

$$\chi = \left[\frac{1}{2} \left((S_{xx})^2 + (S_{yy})^2 + 2(S_{xy})^2 \right) \right]^{\frac{1}{2}}.$$
 (20)

The equations (4)-(8) can be reduced to by using the above parameters with no dimension.

$$\frac{\partial p}{\partial x} = \frac{\partial S_{xy}}{\partial y}, \tag{21}$$

$$\frac{\partial p}{\partial y} = 0, \tag{22}$$

$$(1 + P_r R_d) \frac{\partial^2 \theta}{\partial y^2} - B_r \left(\frac{\partial^2 \psi}{\partial y^2} \right) = 0, \tag{23}$$

$$\frac{\partial^2 \Omega}{\partial y^2} + (S_c S_r) \frac{\partial^2 \theta}{\partial y^2} = 0, \tag{24}$$

$$S_{xx} = 0, \quad S_{yy} = 0, \tag{25}$$

$$S_{xy} = \frac{\frac{\partial^2(\psi)}{\partial y^2}}{1 + (\beta S_{xy})^{\alpha-1}}. \tag{26}$$

Where P_r represents Prandtl number, S_r represents Soret number, B_r Brinkman number, S_c denotes Schmidt number, and R_d denotes the thermal radiation.

Eq. (21) states that (P) is an independent function of (y), and since (P) is only dependent on variable (x), we treat it as a constant in the integration procedure (21). By integrating Eq. (21) for (y) and applying the boundary constraint, we get

$$S_{xy} = \frac{\partial p}{\partial x} y. \tag{27}$$

The boundary conditions with no dimension in the problem's wave frame are

$$\left. \begin{aligned} \frac{\partial^2 \psi}{\partial Y^2} = 0, \quad \theta = 0, \quad \Omega = 0 \quad \text{at} \quad y = 0, \\ \frac{\partial \psi}{\partial Y} = 1, \quad \theta = 1, \quad \Omega = 1 \quad \text{at} \quad y = h = 1 + \frac{K \lambda X}{a} + \phi \sin 2\pi(x-t) - \phi_1 \cos^4 \left(\frac{2\pi}{\lambda_1} \right). \end{aligned} \right\} \tag{28}$$

Consider the average flux q in the wave frame with no dimension, which is given as

$$q = \int_{h_1(x)}^{h_2(x)} \frac{\partial \psi}{\partial y} dy, \tag{29}$$

In wave frame, the mean time is given by $Q = q + 1 + d$.

3. Method of Solution

Using symbolic Mathematica and Ms-DTM, the equations (27, 23 and 24) with the boundary conditions (28) are computed. The detail about the Ms-DTM can be found in the reference [22-31].

$$(k+2)(k+1)\Psi(k+2) - \frac{\partial P}{\partial x} \delta(k-1) + \beta^{\alpha-1} \left(\frac{\partial P}{\partial x} \right)^\alpha \delta(k-\alpha) = 0. \tag{30}$$

$$(k+2)(k+1)\Theta(k+2) - \frac{B_r}{1 + P_r R_d} (k+2)(k+1)\Psi(k+2) = 0. \tag{31}$$

$$(k+2)(k+1)\Phi(k+2) + S_c S_r (k+2)(k+1)\Theta(k+2) = 0. \tag{32}$$

Where $\Psi[k]$, $\Theta[k]$ and $\Phi[k]$ and are the differential transformation functions of $\psi(y)$, $\vartheta(y)$, and $\Omega(y)$ respectively and given as

$$\psi(y) \cong \sum_{k=0}^m \Psi(k)y^k, \tag{33}$$

$$\theta(y) \cong \sum_{k=0}^m \Theta(k)y^k, \tag{34}$$

$$\Omega(y) \cong \sum_{k=0}^m \Phi(k)y^k. \tag{35}$$

The transformed form of boundary constraints are given as $\Psi(0) = m_1, \Psi(1) = m_2, \Psi(2) = 0, \Theta(0) = 0, \Theta(1) = m_3, \Phi(0) = 0, \Phi(1) = m_4$. (36)

where m_4, m_3, m_2 and m_1 are unknown elements that must be determined.

Putting equation (36) into equations (30)-(32) and further values of $\Psi[k], \Theta[k]$ and $\Phi[k]$ can be determined by recursive method. Hence, substitute all $\Psi[k], \Theta[k]$ and $\Phi[k]$ into equations (33)-(35), obtained series solutions are as

$$\psi(y) = m_1 + m_2y + \frac{1}{6} \frac{\partial P}{\partial x} y^3 + \frac{\beta}{12} \frac{\partial P}{\partial x} y^4 + \dots \tag{37}$$

$$\theta(y) = m_3y + \frac{1}{6} \frac{B_r}{(1 + P_r R_d)} \frac{\partial P}{\partial x} y^3 + \frac{1}{12} \frac{\beta B_r}{(1 + P_r R_d)} \frac{\partial P}{\partial x} y^4 + \dots \tag{38}$$

$$\Omega(y) = m_4y - \frac{1}{6} \frac{S_c S_r B_r}{(1 + P_r R_d)} \frac{\partial P}{\partial x} y^3 - \frac{1}{12} \frac{S_c S_r \beta B_r}{(1 + P_r R_d)} \frac{\partial P}{\partial x} y^4 + \dots \tag{39}$$

Differentiating equation (41) partially with respect to y we get the velocity equation as

$$U(y) = m_2 + \frac{1}{2} \frac{\partial P}{\partial x} y^2 + \frac{\beta}{3} \frac{\partial P}{\partial x} y^3 + \dots \tag{40}$$

Using boundary conditions of equation (28) we can obtain the values of m_1, m_2, m_3 and m_4 .
 $m_1 = -0.3301, m_2 = 0.5033, m_3 = 0.98342, m_4 = 1.0165$.

4. Results and Discussion

The study shows the application of viscous dissipation and rough surface effects in peristaltic Ellis liquid movement though non-uniform channel. The results obtained by Ms-DTM have been compared with the results obtained by NDSolve. The results show that they matched nicely as can be seen from Tables 1. Here the development of temperature, velocity and concentration distribution also streamline graphs corresponding to variation of Ellis fluid parameter β , parameter of wall rigidity E_1 , parameter of wall tension E_2 , parameter of mass characterization E_3 , Thermal radiation R_d , Schmidt number S_c , Brinkman number B_r , Prandtl number P_r and Soret number S_r are discussed.

4.1. Velocity Profile

The effects of β, E_1, E_2 and E_3 on velocity distribution $u(y)$ are shown through figures 2 to 5. In Fig.2, velocity near the centre of channel enhances with rising β on the contrary, it follows the inverse trend near the channel wall. Fig. 3 and Fig. 4 demonstrates the behavior of parameter of wall rigidity E_1 and parameter of wall tension E_2 respectively. Velocity in peristaltic pumping decreases with an increase in parameter of wall rigidity E_1 it follows the inverse trend near the channel wall. Similar behavior is seen in parameter of wall tension E_2 . Fig. 5 shows the velocity in peristaltic

pumping rises with a rise in parameter of Mass characterization E_3 it follows the inverse trend near the channel wall.

4.2. Temperature Profile

Figures 6 to 9 demonstrates the temperature profile through β , B_r , P_r and R_d . Fig. 7 shows that temperature distribution diminishes when there is a rise in Brinkman number B_r . Fig. 6 demonstrates that the temperature distribution enhances when there is a rise in Ellis fluid parameter β . Fig. 8 demonstrates that the temperature distribution enhances when there is a rise in Prandtl number P_r . Physically, low Prandtl numbers indicate high heat diffusivity, while high Prandtl numbers indicate progressive momentum. The Prandtl number is always positive to control the force and thermal boundary layer thickness. Fig. 9 demonstrates that the temperature distribution enhances when there is a rise in Thermal radiation R_d . When the radiation parameter increases, it improves the movement of electromagnetic waves while suffocating heat conduction. Because dispersion heat exchange occurs as a result of irregular atom proliferation, when it is extinguished, the neighbouring particles spread less, and the vitality exchange rate between them becomes less productive. Furthermore, diffusive heat exchange has a longer time scale than radiative heat exchange.

4.3 Concentration Profile

Figures 10 to 13 demonstrates the concentration distribution influenced by Ellis fluid parameter β , Schmidt number S_c , Brinkman number B_r and Soret number S_r . Fig.10 shows that as an Ellis fluid parameter β rises the concentration profile diminishes. Fig.11 shows that solutal concentration profile in peristaltic pumping increases by rising the values of B_r . Fig.12 demonstrates the solutal concentration profile in peristaltic flow increases by rising the values of S_c . Schmidt number S_c have an increasing effect on concentration. Schmidt number S_c is a rate of viscous diffusion to molecular diffusion. Hence, a greater Schmidt number S_c enhances the rate of viscous diffusion. Fig.13 shows that solutal concentration profile in peristaltic transport increases by increasing the values of S_r . The ratio of the thermodiffusion coefficient to the diffusion coefficient is known as the Soret number.

4.4 Trapping Phenomenon

Figures 14 to 17 demonstrate that the streamlines influenced by β , E_1 , E_2 and E_3 . Basically, trapping is the creation of internally circulating bolus. The volume of the bolus is defined as the fluid bounded by the closed streamlines. Fig.14 shows that an Ellis fluid parameter β rises then the magnitude of the bolus is increased. Fig.15 shows that as wall rigidity parameter E_1 rises strength of trapped bolous observed in the wider part of the channel diminishes. Fig.16 shows that as wall tension parameter E_2 rises strength of trapped bolous observed in the wider part of the channel decreases. Fig.17 shows that as Mass characterization parameter E_3 rises the strength of the trapped bolous in the wider part of the channel is decreasing.

Table 1

Comparison of the solution obtained by Ms-DTM with the NDSolve for $E_1 = 0.001, E_2 = 0.01, E_3 = 0.01, \phi = 0.8, \phi_1 = 0.016, \beta = 0.1, \lambda = 0.1, \lambda_1 = 0.1, a = 0.1, x = 0.75, t = 0.2, k = 0.005, F = 0.25$.

y	Velocity	NDSolve	Temperature	NDSolve	Concentration	NDSolve
0	0.143353	0	0.	0	0.	0
0.2	0.182485	0.18248	0.198057	0.19805	-0.00136615	-0.001366
0.4	0.300091	0.30009	0.406886	0.40688	0.01568	0.01568
0.6	0.496482	0.49648	0.64423	0.64423	0.114941	0.11494
0.8	0.771971	0.77197	0.935436	0.93543	0.402757	0.40275
1	1.012687	1	1.01345	1	1.028	1

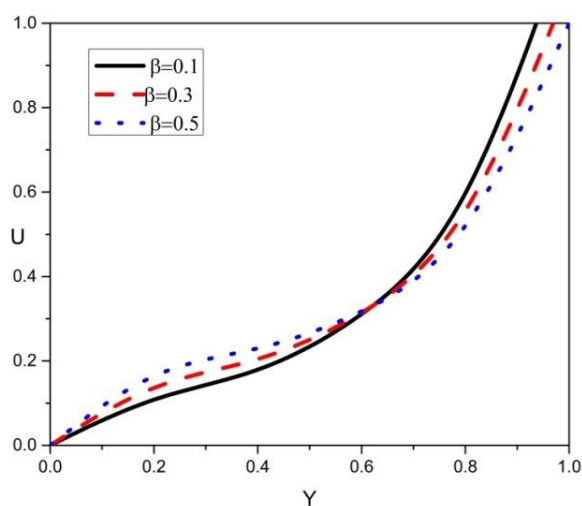


Fig. 2. Influence of β on distribution of Velocity
 $E_1 = 0.001, E_2 = 0.01, E_3 = 0.01, \phi = 0.8, \phi_1 = 0.016,$
 $\lambda = 0.1, \lambda_1 = 0.1, a = 0.1, x = 0.75, t = 0.2, k = 0.005, F = 0.25$.

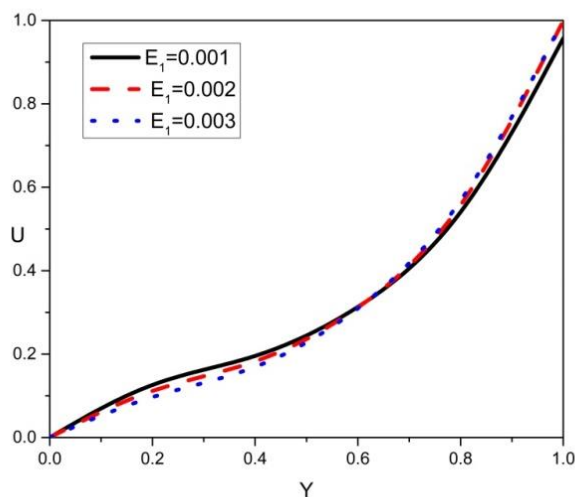


Fig. 3. Influence of E_1 on distribution of Velocity
 $\beta = 0.1, E_2 = 0.01, E_3 = 0.01, \phi = 0.8, \phi_1 = 0.016,$
 $\lambda = 0.1, \lambda_1 = 0.1, a = 0.1, x = 0.75, t = 0.2, k = 0.005, F = 0.25.$

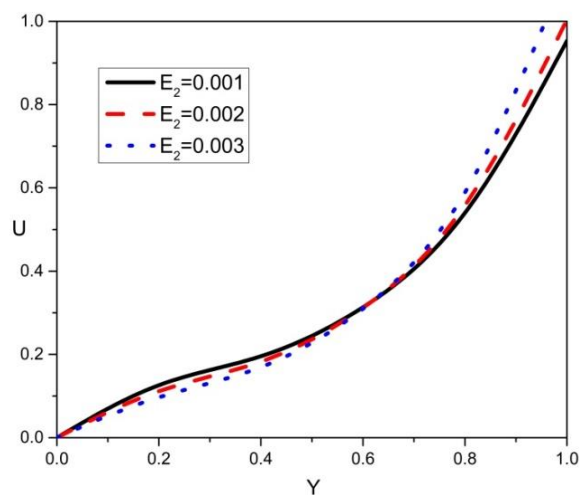


Fig. 4. Influence of E_2 on distribution of Velocity
 $\beta = 0.1, E_1 = 0.001, E_3 = 0.01, \phi = 0.8, \phi_1 = 0.016,$
 $\lambda = 0.1, \lambda_1 = 0.1, a = 0.1, x = 0.75, t = 0.2, k = 0.005, F = 0.25.$

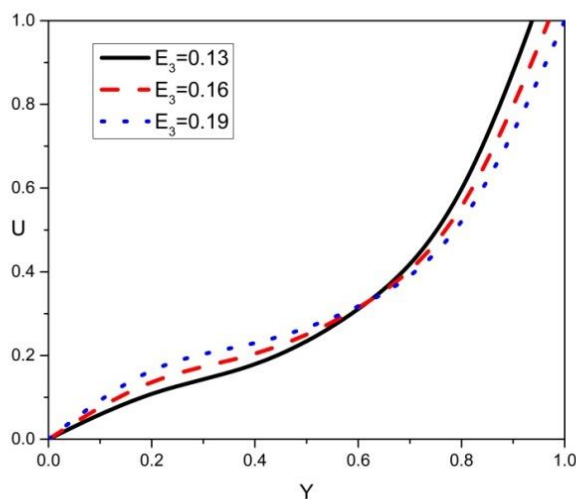


Fig. 5. Influence of E_3 on distribution of Velocity
 $\beta = 0.1, E_1 = 0.001, E_2 = 0.01, \phi = 0.8, \phi_1 = 0.016,$
 $\lambda = 0.1, \lambda_1 = 0.1, a = 0.1, x = 0.75, t = 0.2, k = 0.005, F = 0.25.$

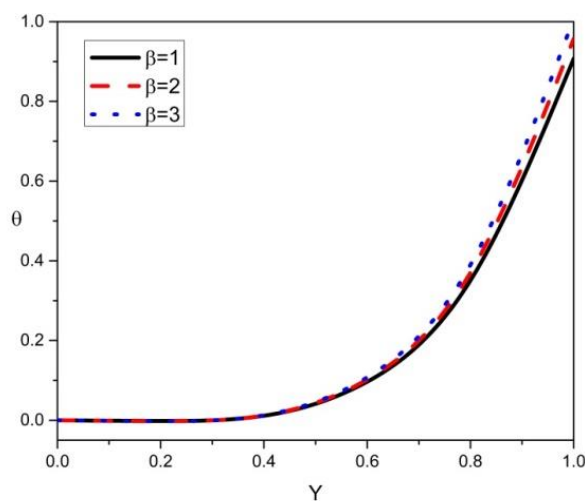


Fig. 6. Influence of β on distribution of Temperature
 $B_r = 0.1, E_1 = 0.001, \phi = 0.8, E_2 = 0.01, \phi_1 = 0.016, E_3 = 0.01, P_r = .1$
 $\lambda = 0.1, \lambda_1 = 0.1, a = 0.1, x = 0.75, t = 0.2, k = 0.005, F = 0.25, R_d = 0.5.$

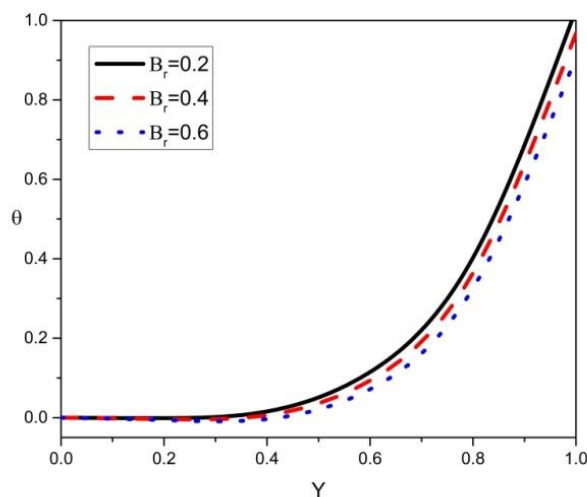


Fig. 7. Influence of B_r on distribution of Temperature
 $\beta = 1, E_1 = 0.001, \phi = 0.8, E_2 = 0.01, \phi_1 = 0.016, E_3 = 0.01, P_r = .1$
 $\lambda = 0.1, \lambda_1 = 0.1, a = 0.1, x = 0.75, t = 0.2, k = 0.005, F = 0.25, R_d = 0.5.$

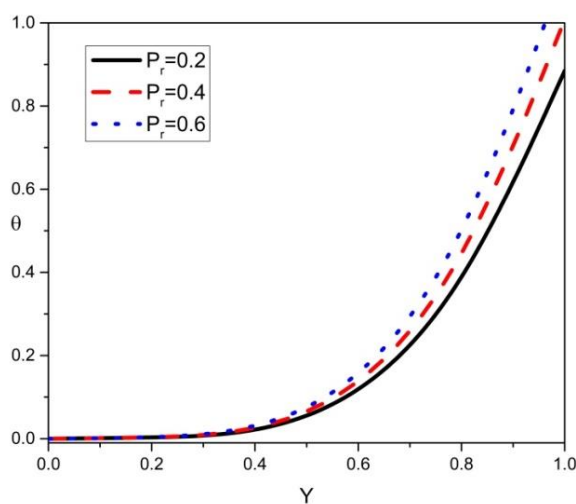


Fig. 8. Influence of P_r on distribution of Temperature
 $\beta = 1, E_1 = 0.001, \phi = 0.8, E_2 = 0.01, \phi_1 = 0.016, E_3 = 0.01, B_r = 0.1$
 $\lambda = 0.1, \lambda_1 = 0.1, a = 0.1, x = 0.75, t = 0.2, k = 0.005, F = 0.25, R_d = 0.5.$

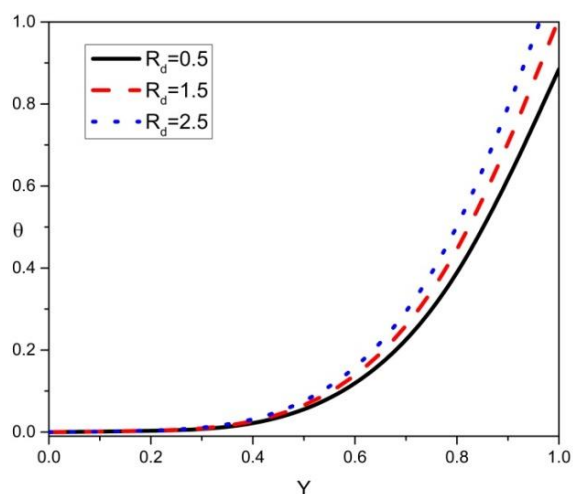


Fig. 9. Impact of R_d on distribution of Temperature
 $\beta = 1, E_1 = 0.001, \phi = 0.8, E_2 = 0.01, \phi_1 = 0.016, E_3 = 0.01, P_r = B_r = 0.1$
 $\lambda = 0.1, \lambda_1 = 0.1, a = 0.1, x = 0.75, t = 0.2, k = 0.005, F = 0.25..$

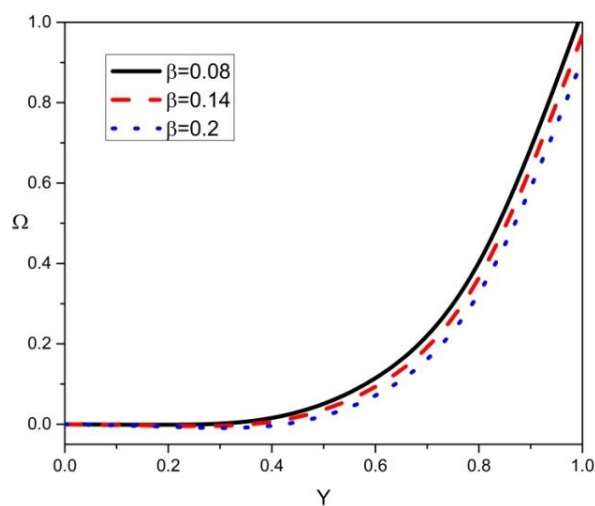


Fig. 10. Impact of β on distribution of Concentration
 $B_r = 1.5, E_1 = 0.001, \phi = 0.8, E_2 = 0.01, \phi_1 = 0.016, E_3 = 0.01, S_r = 1.5, S_c = 1,$
 $\lambda = 0.1, \lambda_1 = 0.1, a = 0.1, x = 0.75, t = 0.2, k = 0.005, F = 0.25, R_d = 0.5, P_r = .1, .$

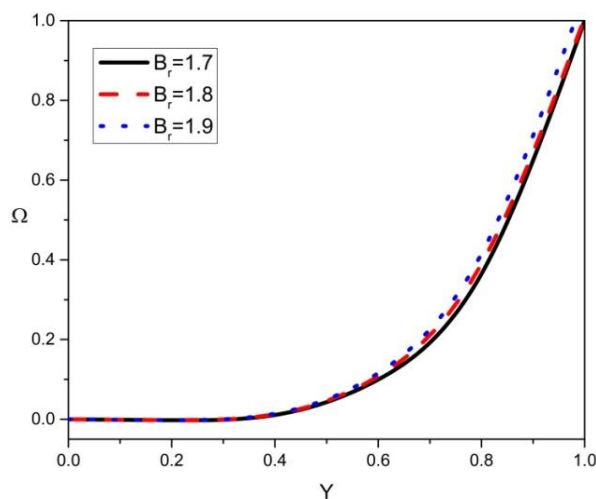


Fig. 11. Impact of B_r on distribution of Concentration

$\beta = 0.1, E_1 = 0.001, \phi = 0.8, E_2 = 0.01, \phi_1 = 0.016, E_3 = 0.01, S_r = 1.5, S_c = 1,$
 $\lambda = 0.1, \lambda_1 = 0.1, a = 0.1, x = 0.75, t = 0.2, k = 0.005, F = 0.25, R_d = 0.5, P_r = 0.1, .$

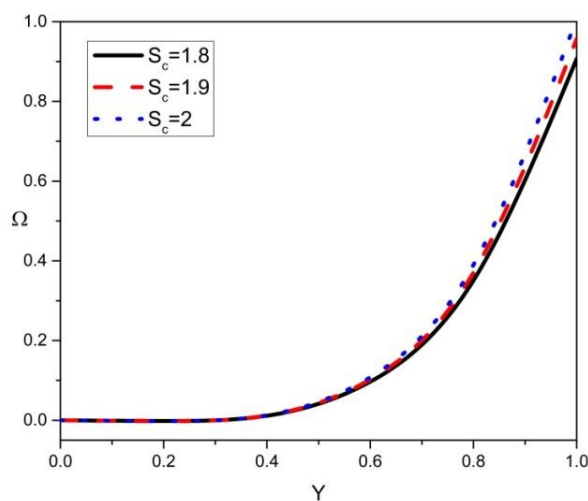


Fig. 12. Impact of S_c on distribution of Concentration

$\beta = 0.1, E_1 = 0.001, \phi = 0.8, E_2 = 0.01, \phi_1 = 0.016, E_3 = 0.01, S_r = 1.5, B_r = 1.5,$
 $\lambda = 0.1, \lambda_1 = 0.1, a = 0.1, x = 0.75, t = 0.2, k = 0.005, F = 0.25, R_d = 0.5, P_r = 0.1, .$

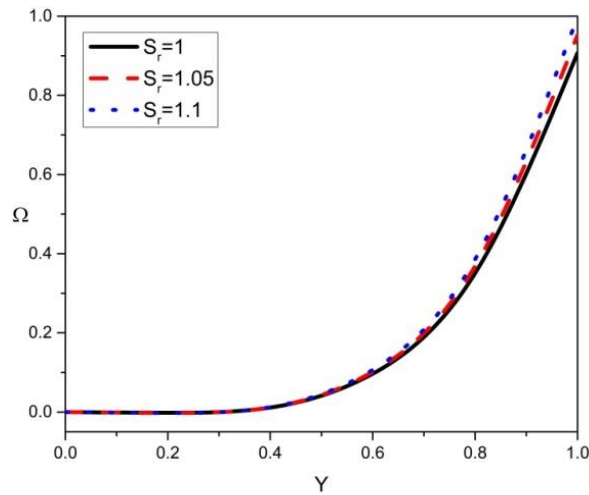


Fig. 13. Impact of S_r on distribution of Concentration
 $\beta = 0.1, E_1 = 0.001, \phi = 0.8, E_2 = 0.01, \phi_1 = 0.016, E_3 = 0.01, S_c = 1, B_r = 1.5,$
 $\lambda = 0.1, \lambda_1 = 0.1, a = 0.1, x = 0.75, t = 0.2, k = 0.005, F = 0.25, R_d = 0.5, P_r = 0.1, .$

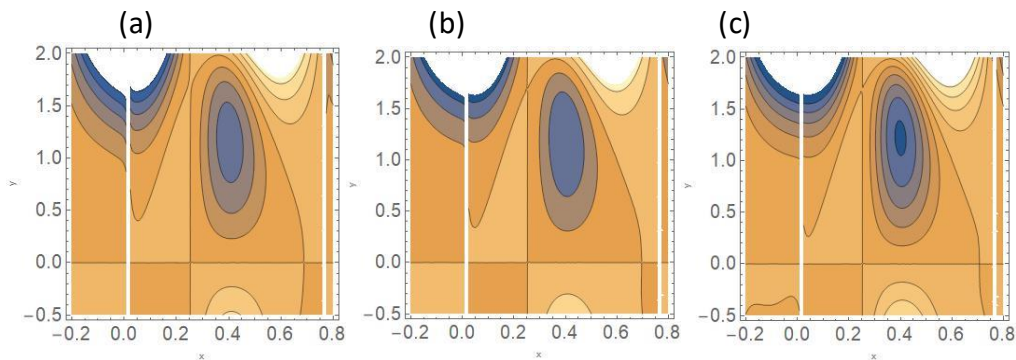


Fig. 14. Streamlines for (a) $\beta = 1$, (b) $\beta = 5$, (c) $\beta = 20$
 $E_1 = 0.001, \phi = 0.8, E_2 = 0.01, \phi_1 = 0.016, E_3 = 0.01,$
 $\lambda = 0.1, \lambda_1 = 0.1, a = 0.1, x = 0.75, t = 0.2, k = 0.005, F = 0.25.$

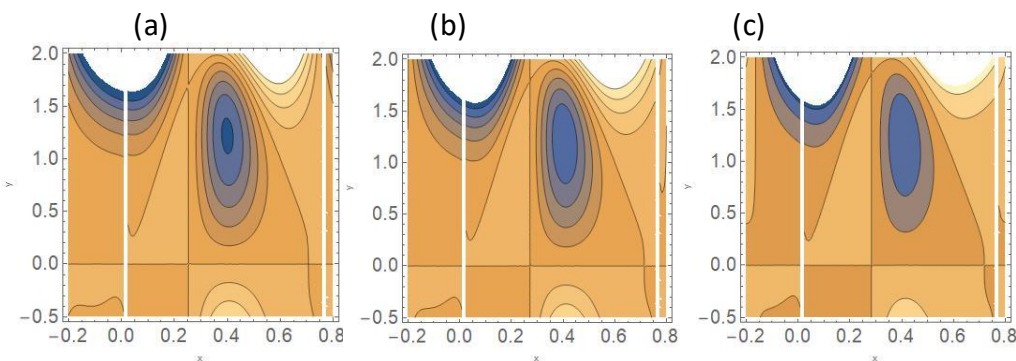


Fig. 15. Streamlines for (a) $E_1 = 0.1$, (b) $E_1 = 0.2$, (c) $E_1 = 0.3$
 $\beta = 0.1, E_2 = 0.01, \phi = 0.8, E_3 = 0.01, \phi_1 = 0.016,$
 $\lambda = 0.1, \lambda_1 = 0.1, a = 0.1, x = 0.75, t = 0.2, k = 0.005, F = 0.25.$

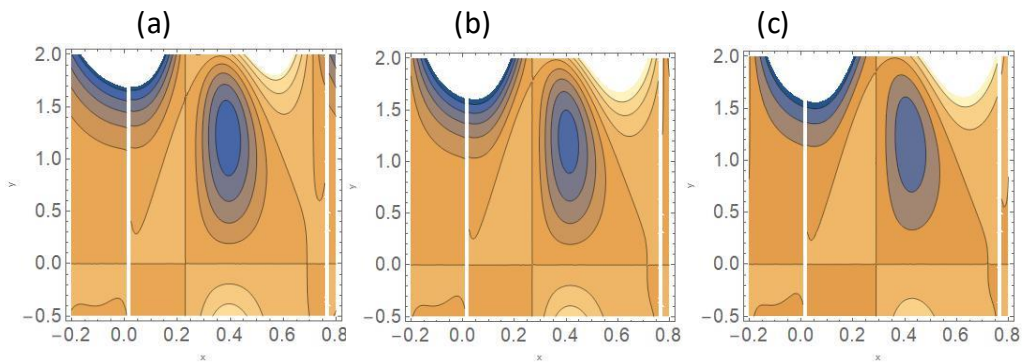


Fig. 16. Streamlines for (a) $E_2 = 0.1$, (b) $E_2 = 0.3$, (c) $E_2 = 0.5$
 $\beta = 0.1, E_1 = 0.001, \phi = 0.8, E_3 = 0.01, \phi_1 = 0.016,$
 $\lambda = 0.1, \lambda_1 = 0.1, a = 0.1, x = 0.75, t = 0.2, k = 0.005, F = 0.25.$

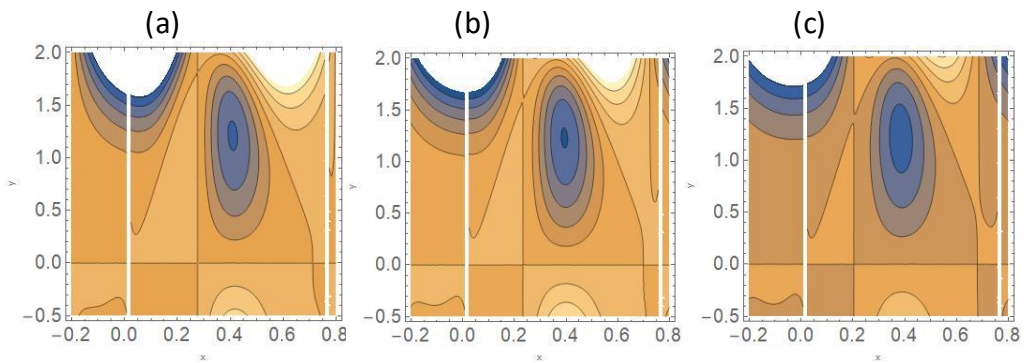


Fig. 17. Streamlines for (a) $E_3 = 1$, (b) $E_3 = 2$, (c) $E_3 = 3$
 $\beta = 0.1, E_1 = 0.001, \phi = 0.8, E_2 = 0.01, \phi_1 = 0.016,$
 $\lambda = 0.1, \lambda_1 = 0.1, a = 0.1, x = 0.75, t = 0.2, k = 0.005, F = 0.25.$

5. Conclusion

This study reports the different predictions about the effect of viscous dissipation features and rough surface on the peristalsis of an Ellis fluid through a non-uniform channel. Non-linear governing equations are solved by using Ms-DTM.

The followings are the main findings of the paper:

- It shows that velocity near the centre of channel enhances with rising Ellis fluid parameter β on the contrary, it follows the inverse trend near the channel wall. Similar behavior is seen in Mass characterization parameter E_3 .
- It is observed that velocity in peristaltic pumping decreases with an increase in wall rigidity parameter E_1 it follows the inverse trend near the channel wall. Similar behavior is seen in wall tension parameter E_2 also.
- Temperature distribution diminishes when there is a rise in Brinkman number B_r .
- Ellis fluid parameter β , Prandtl number P_r and Thermal radiation R_d have similar behavior in temperature distribution.
- Ellis fluid parameter β rises the concentration profile diminishes.

- It is observed that B_r , S_c and S_r have similar behavior in concentration profile.
- an Ellis fluid parameter β rises then the magnitude of the bolus is increased
- Wall rigidity parameter rises strength of trapped bolous observed in the wider part of the channel diminishes. Similar behavior is seen in wall tension parameter E_2 and in Mass characterization parameter E_3 .

Acknowledgement

Author Joonabi Beleri would like to thank Directorate of Minorities for their financial support [DOMWDD/Ph.D//FELLOWSHIP/CR-01/2019-20] Date: 15.10.2019.

References

- [1] Latham, T. "Motion in a peristaltic pump." PhD diss., MS thesis, ed: MIT-Press, Cambridge, Mass, USA, 1966.
- [2] Shapiro, Ascher H., Michel Yves Jaffrin, and Steven Louis Weinberg. "Peristaltic pumping with long wavelengths at low Reynolds number." *Journal of fluid mechanics* 37, no. 4 (1969): 799-825.
- [3] Jaffrin, M. Y., and A. H. Shapiro. "Peristaltic pumping." *Annual review of fluid mechanics* 3, no. 1 (1971): 13-37.
- [4] Asha, S. K., and G. Sunita. "Effect of couple stress in peristaltic transport of blood flow by homotopy analysis method." *AJST* 12 (2017): 6958-6964.
- [5] Gajbhare, Bhi manand Pandurang, Krishna Prasad JSVR, and S. R. Mishra. "Peristaltic pumping through non-Darcy porous medium in an electroosmotic flow with entropy analysis." *Nano system, Physics, Chemistry* 11, no. 4 (2020): 379-390.
- [6] Longwell, Paul A. *Mechanics of fluidflow*. McGraw-Hill, 1966.
- [7] Imran, Naveed, Asifa Tassaddiq, Maryiam Javed, Nasser Aedh Alreshidi, Muhammad Sohail, and Ilyas Khan. "Influence of chemical reactions and mechanism of peristalsis for the thermal distribution obeying slip constraints: Applications to conductive transportation." *Journal of Materials Research and Technology* 9, no. 3 (2020): 6533-6543.
- [8] Abbas, M. Ali, M. M. Bhatti, and M. M. Rashidi. "Peristaltic blood flow of Ellis fluid through a nonuniform channel having compliant Walls." *Journal of Nanofluids* 6, no. 2 (2017): 318-323.
- [9] Ali, N., A. Abbasi, and I. Ahmad. "Channel flow of Ellis fluid due to peristalsis." *AIP Advances* 5, no. 9 (2015): 097214.
- [10] Saravana, R., S. Sreenadh, P. Rajesh Kumar, and V. Ramesh Babu. "Peristaltic pumping of Ellis fluid through a flexible tube with complete slip effects." *Journal of Naval Architecture and Marine Engineering* 17, no. 2 (2020): 79-88.
- [11] Ali, N., S. Hussain, K. Ullah, and O. Anwar Bég. "Mathematical modelling of two-fluid electro-osmotic peristaltic pumping of an Ellis fluid in an axisymmetric tube." *The European Physical Journal Plus* 134, no. Apr 19 (2019): 141.
- [12] Goud, J. Suresh, and R. Hemadri Reddy. "Peristaltic motion of an Ellis fluid model in a vertical uniform tube with wall properties." *International Journal of Civil Engineering and Technology* 9 (2018): 847-856.
- [13] Goud, J. Suresh, Pudhari Srilatha, L. Indira, B. Raju, and A. Praveen. "peristaltic motion of an ellis fluid model in a vertical uniform tube with wall properties and slip condition." *Journal of Natural Remedies* 21, no. 5 (S2) (2020): 18-27.
- [14] Kumar, K. Thanesh, A. Kavitha, and R. Saravana. "Peristaltic flow of an Ellis fluid model in an inclined uniform tube with wall properties." *International Journal of Mechanical Engineering and Technology* 9, no. 2 (2018): 15-27.
- [15] Shukla, R., A. Medhavi, S. S. Bhatt, and R. Kumar. "Mathematical Analysis of Heat Transfer in Peristaltic Transport through a Rough Nonuniform Inclined Channel." *Mathematical Problems in Engineering* 2020 (2020).
- [16] Shukla, R., S. S. Bhatt, A. Medhavi, and R. Kumar. "Effect of Surface Roughness during Peristaltic Movement in a Nonuniform Channel." *Mathematical Problems in Engineering* 2020 (2020).
- [17] Burton, Hanna E., and Daniel M. Espino. "The effect of mechanical overloading on surface roughness of the coronary arteries." *Applied bionics and biomechanics* 2019 (2019).
- [18] Taylor, James B., Andres L. Carrano, and Satish G. Kandlikar. "Characterization of the effect of surface roughness and texture on fluid flow—past, present, and future." *International journal of thermal sciences* 45, no. 10 (2006): 962-968.
- [19] Shaheen, Aqila, and Muhammad Imran Asjad. "Peristaltic flow of a Sisko fluid over a convectively heated surface with viscous dissipation." *Journal of Physics and Chemistry of Solids* 122 (2018): 210-217.
- [20] Mehmood, Obaid Ullah, Norzieha Mustapha, and Sharidan Shafie. "Peristaltically Induced Flow of Fourth Grade Fluid with Viscous Dissipation." *WASJ* 21 (2013): 36-141.

- [21] Abou-Zeid, Mohamed. "Effects of thermal-diffusion and viscous dissipation on peristaltic flow of micropolar non-Newtonian nanofluid: application of homotopy perturbation method." *Results in Physics* 6 (2016): 481-495.
- [22] Zhou, J. K. "Differential transformation and its applications for electrical circuits." (1986): 1279-1289.
- [23] Odibat, Zaid M., Cyrille Bertelle, M. A. Aziz-Alaoui, and Gérard HE Duchamp. "A multi-step differential transform method and application to non-chaotic or chaotic systems." *Computers & Mathematics with Applications* 59, no. 4 (2010): 1462-1472.
- [24] Hasona, Wahed M., Abdelhafeez El-Shehkipy, and M. G. Ibrahim. "Semi-analytical solution to MHD peristaltic flow of a Jeffrey fluid in presence of Joule heat effect by using multi-step differential transform method." *New Trends in Mathematical Sciences* 7, no. 2 (2019): 123-137.
- [25] Hasona, W. M. "Temperature-dependent electrical conductivity and thermal radiation effects on MHD peristaltic motion of Williamson nanofluids in a tapered asymmetric channel." *Journal of Mechanics* 36, no. 1 (2020): 103-118.
- [26] Hasona, W. M., A. A. El-Shehkipy, and M. G. Ibrahim. "Combined effects of magnetohydrodynamic and temperature dependent viscosity on peristaltic flow of Jeffrey nanofluid through a porous medium: Applications to oil refinement." *International Journal of Heat and Mass Transfer* 126 (2018): 700-714.
- [27] Tripathi, Dharmendra, Osman Anwar Bég, Praveen Kumar Gupta, Ganjam Radhakrishnamacharya, and Jagannath Mazumdar. "DTM simulation of peristaltic viscoelastic biofluid flow in asymmetric porous media: a digestive transport model." *Journal of Bionic Engineering* 12, no. 4 (2015): 643-655.
- [28] Hatami, Mohammad, Seyed Ebrahim Ghasemi, S. A. R. Sahebi, Sobhan Mosayebidorcheh, D. D. Ganji, and Javad Hatami. "Investigation of third-grade non-Newtonian blood flow in arteries under periodic body acceleration using multi-step differential transformation method." *Applied Mathematics and Mechanics* 36, no. 11 (2015): 1449-1458.
- [29] Bég, O. Anwar, M. Keimanesh, M. M. Rashidi, M. Davoodi, and South Tehran Branch. "Multi-Step DTM simulation of magneto-peristaltic flow of a conducting Williamson viscoelastic fluid." *Int. J. Appl. Math. Mech* 9, no. 6 (2013): 1-19.
- [30] Kotnurkar A. S, Beleri J, Badruddin I. A, Kamangar S, Ahammad N. A. "Peristaltic Transport of Carreau Nanofluid in Presence of Triple Diffusion in an Asymmetric Channel by Multi-Step Differential Transformation Method." *Mathematics* 10, no. 5 (2022): 807.
- [31] Asha, S. K., and Joonabi Beleri. "Peristaltic flow of Carreau nanofluid in presence of Joule heat effect in an inclined asymmetric channel by multi-step differential transformation method." *World Scientific News* 164 (2022): 44-63.